Article

Monitoring of Photovoltaic System Performance Using Outdoor Suns-V_{OC}

Alexander C. Killam, Joseph F. Karas, André Augusto, Stuart G. Bowden

alexander.killam@asu.edu (A.C.K.)
joseph.f.karas@asu.edu (J.F.K.)
augusto@asu.edu (A.A.)
sgbowden@asu.edu (S.G.B.)

HIGHLIGHTS

Extracted outdoor Suns-V_{OC} parameters fall within 1% of indoor lab measurements

Weather station data proved as a scalable alternative to individual sensors

Suns-V_{OC} parameters can be extracted at low irradiance periods (i.e., sunrise)

This method is resilient to instances of partial shading or cloud coverage

Photovoltaics have historically been warrantied for 25 years, but a recent push is being made to extend lifespans to 50 years. Data must be collected on fielded systems to better understand degradation mechanisms and impacts from different climates. We show how Suns-V_{OC}, a widely used method for indoor characterization, can be used to collect data on fielded modules without impeding power production. This methodology can be applied to systems of all sizes and provide analysis of impeding faults and degradation.

Article

Monitoring of Photovoltaic System Performance Using Outdoor Suns-V$_{OC}$

Alexander C. Killam,[1,2,*] Joseph F. Karas,[1,*] André Augusto,[1,*] and Stuart G. Bowden[1,*]

SUMMARY

In-field characterization of photovoltaics is crucial to understand performance and degradation mechanisms, subsequently improving overall reliability and lifespans. Current outdoor characterization is limited by logistical difficulties, variable weather, and requirements to measure during peak production hours. We capitalize on Suns-V$_{OC}$, which is widely used for laboratory measurements of single solar cells and discuss the barriers in extending the technique to outdoor systems. We demonstrate the normalization of measurements using both backsheet temperature sensors and on-site weather stations. Despite weather variation, V$_{OC}$, ideality factor, and pseudo fill factor all fall within 1% of the laboratory measurements. It is also demonstrated that monitoring the system V$_{OC}$ at 0.05 to 0.1 suns, during minimal power production, provides a figure of merit that can indicate early degradation of the system. Extensive simulations show that shading portions of a system has minimal effect on measurements, allowing the technique to be used in all weather conditions.

INTRODUCTION

Maintaining high performance fielded photovoltaic (PV) systems requires adequate and informative characterization tools. In-field characterization methods are an essential part of performance monitoring,[1] system diagnostics/detection, and attribution of premature component failure.[2] Monitoring changes in power output has historically been used to gauge levels of degradation, but it fails to provide insight on specific loss mechanisms.[3,4] Indoor Suns-V$_{OC}$ has been used extensively to identify and quantify loss mechanisms as well as identify the early onset of losses such as resistive shunts[5] during reliability testing. In this work, we demonstrate the scalability of using outdoor Suns-V$_{OC}$ as a complementary or alternative characterization technique for monitoring modules and arrays, requiring minimal hardware, and utilizing the sun as the illumination source without impeding power production. The implications of this work can be used to better understand the operation of systems of all sizes, ranging from small residential systems to larger powerplant sized systems. We also demonstrate that this method is robust for systems operating under partial shading conditions.

At the end of 2019, 650 GW of PV was installed throughout the world, representing over 2 billion panels operating in multiple climates with varying weather conditions.[6] In 2024, projections show this number doubling. For many of these systems, the only available performance metrics are based on power output measurements. Small, distributed systems of heterogeneous design and configuration may not be well characterized enough for inclusion in large fleet-scale performance datasets.[7] Power-based performance metrics are clearly insufficient given variable weather conditions and high DC to AC ratios, and they do not provide insight into specific

Context & Scale

Photovoltaics (PVs) have rapidly grown due to advancements in efficiency and cost. PV is projected to increase to 48% of all renewable generation by 2050, making it the fastest growing source of energy generation. More emphasis has been placed on reliability, as a path to reducing LCOE by improving degradation rates and system lifespans.

We capitalize on Suns-V$_{OC}$, which is widely used for laboratory measurements of single solar cells, and discuss the barriers in extending the technique to outdoor systems of all sizes. The resulting data can provide a thorough analysis of impeding faults and degradation. Because Suns-V$_{OC}$ is rather simple to implement on fielded systems, it can be a valuable tool for collecting the data needed to better understand how degradation mechanisms and climates impact different PV architectures. This work provides a scalable pathway to provide the industry with the information needed to achieve PV lifespans of beyond 50 years.

Table 1. Detection of Common Degradation Mechanisms of Fielded PV Modules

Degradation Mechanism	Degradation Cause	Resulting Performance	Potential Characterization Method
Solder joint failure	Thermal	R_S increase	R_S from Suns-V_{OC}[9]
Delamination/discoloration (resulting in corrosion)	Moisture, Thermal, UV	I_{SC} reduction, R_S increase	Physical Inspection/R_S from Suns-V_{OC}[9]
LID	Irradiance	I_{SC} & V_{OC} reduction	Suns-V_{OC}[10]
LeTID	Irradiance, Tthermal	I_{SC} & V_{OC} reduction	Suns-V_{OC}[11]
PID	Voltage	I_{SC} & R_{SH} reduction	Suns-V_{OC}[12]

mechanisms for power decline. Small and large systems alike would benefit from scalable, real-time performance metrics more robust to variable conditions that provide mechanistic insight into system performance, degradation, and failures.[8]

PV systems may suffer from various degradation mechanisms, influenced by cell and module architecture, installation, and local weather and climate. Some common degradation mechanisms, which can be evaluated and attributed with Suns-V_{OC} or the extracted series resistance (R_S) from Suns-V_{OC},[9] are listed in Table 1. Suns-V_{OC}, especially if complemented with other characterization, can provide attribution of degradation mechanisms that affect system current-voltage (I-V) properties, including short circuit current (I_{SC}), open-circuit voltage (V_{OC}), R_S, shunt resistance (R_{SH}), etc.

Using Suns-V_{OC}, many of the most common degradation mechanisms can be detected. Most of the referenced work in Table 1 uses indoor Suns-V_{OC} measurements at the cell level. Outdoor Suns-V_{OC} measurements on large systems have the potential to provide the same metrics as indoor Suns-V_{OC}, enabling observations of these same degradation mechanisms in fielded modules. Suns-V_{OC} offers an alternative to power-based performance data and is relatively simple to implement on systems of all sizes. We believe that by implementing Suns-V_{OC} on outdoor systems, the PV community can begin collecting more datasets on systems of different sizes, cell types, and climates, effectively providing the data needed for more thorough reliability and degradation analyses.

Current techniques of acquiring data tend to only provide data at maximum power points and can pose difficulties for scaling to larger plants. I-V curves are a common method for in-field characterization of diode properties but can create logistical difficulties in large fields, such as disconnecting and reconnecting modules, or acquiring enough measurements to provide an accurate statistical representation of the overall system. These logistical difficulties interrupt power production during measurements and prevent scalability. Novel techniques, such as characterization using aerial imaging, provide scalable alternatives to the logistical complications of I-V measurements, but these methods are not able to measure circuit parameters.[13] Furthermore, power or I-V analysis is typically restricted to unshaded, clear sky periods, meaning that data from systems with persistent shade or poor prevailing irradiance are either excluded from large fleet-scale analyses[14] or requires statistical translations of data from shaded conditions to hypothetical clear sky conditions.[7] Here, we present a direct measurement, Suns-V_{OC}, that is relatively simple to collect, can be collected at times of low irradiance, and is robust to partial shading.

[1]School of Electrical, Computer and Energy Engineering, Arizona State University, Tempe, AZ 85287, USA

[2]Lead Contact

*Correspondence:
alexander.killam@asu.edu (A.C.K.),
joseph.f.karas@asu.edu (J.F.K.),
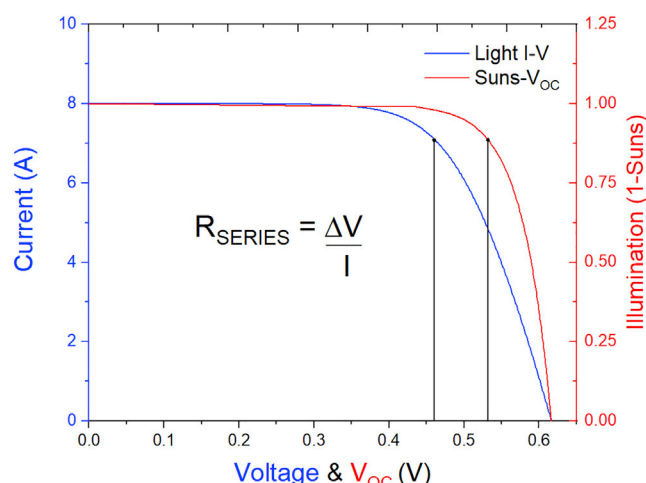augusto@asu.edu (A.A.),
sgbowden@asu.edu (S.G.B.)

Figure 1. Light I-V and Suns-V$_{OC}$ Curves
Comparison of simulated light I-V and Suns-V$_{OC}$ for a typical silicon solar cell.

Suns-V$_{OC}$ has previously been demonstrated outdoors on modules and arrays,[15–18] but without details regarding day-to-day variation and impacts from uncontrollable weather. Variations include transient, diurnal, and seasonal effects like cloud coverage,[19] temperature changes,[20] wind,[21] angle-of-incidence changes,[22] spectral effects,[23] albedo,[24] and soiling.[25] Robust characterization techniques must be able to normalize data obtained in changing conditions. Temperature is the most crucial variable in this study due to the drastic impact it has on PV's V$_{OC}$. Temperature variation is also the biggest difference between indoor and outdoor measurements, and the ability to correct for temperature enables the use of the existing literature base in Suns-V$_{OC}$. In this work, we show how to use Suns-V$_{OC}$ in outdoor conditions, by normalizing the temperature effects during measurements using both backsheet and ambient temperature.

Irradiance effects, such as spectrum shifts, are of secondary importance since the V$_{OC}$ varies with the logarithm of the light intensity, and the irradiance sensor has the same characteristics as the array. Indeed, we show below that the gross effect of shading has a minimal effect on the Suns-V$_{OC}$ measurements.

Suns-V$_{OC}$ allows the construction of a pseudo I-V curve (Figure 1), which is equivalent to the standard I-V curve described above but without the effects of R$_S$.[5] The measurement provides estimations of recombination-related parameters that limit the fill factor (FF), which are difficult to discern from light I-V curves alone.[26,27] Suns-V$_{OC}$ provides the following parameters: the Suns-V$_{OC}$ curve maximum power point and fill factor, i.e., pseudo max power and pseudo FF (pP$_{MP}$ and pFF), two-diode parameters fitted to the Suns-V$_{OC}$ curve (J$_{01}$ and J$_{02}$), and diode ideality factor (n) as a function of cell operating point.

In addition to the parameters derived directly from the Suns-V$_{OC}$ curve in the previous paragraph, comparing the light I-V curve with the Suns-V$_{OC}$ curve (Figure 1) enables the accurate measurement of R$_S$, given by Equation 1:

$$R_S = \frac{\Delta V}{I},$$ (Equation 1)

where ΔV is the voltage difference between the corresponding Suns-V$_{OC}$ and the light I-V curve, and I is the current. In this paper, we present V$_{OC}$ at 1 and 0.1

Table 2. STC Ratings of BSM230 PV Modules

Module Electrical Parameter	Nominal Values
P_{MP}	230 ($\pm$ 5%) W
I_{MP}	4.82 ($\pm$ 5%) A
V_{MP}	48.05 ($\pm$ 5%) V
I_{SC}	5.23 ($\pm$ 5%) A
V_{OC}	58.6 ($\pm$ 5%) V

suns, pP_{MP}, and pFF, but other parameters might also be of interest, particularly for attribution of degradation mechanisms.[28]

Indoor Suns-V_{OC} uses a slowly varying-intensity light source to excite the cell over several orders of magnitude of irradiance.[29] The irradiance is measured in Suns, a convenience unit to describe fractions of 1 kW/m^2. Outdoors, the diurnal changes in the solar insolation (including just before sunrise and just after sunset) provide the required changes in light intensity. The most critical point in a Suns-V_{OC} measurement corresponds to the maximum power point (M_{PP}) on the one-sun I-V power curve. Since the voltage across the diode is the same in both cases, the excess carrier concentrations are roughly equivalent, even though the Suns-V_{OC} measurement is at open-circuit while the M_{PP} is under load. The equivalence in operating points means they have the same levels of recombination, and quantifying losses in the Suns-V_{OC} measurement applies directly to the IV curve. The illumination in suns required to capture information about M_{PP}, Suns(M_{PP}) is related to one-sun I_{SC} and I_{MP} by Equation 2:

$$Suns(M_{PP}) = \frac{I_{SC} - I_{MP}}{I_{SC}}$$

(Equation 2)

Based on the CEC database,[30] the Suns(M_{PP}) for roughly 95% of commercial silicon modules falls within the range of 0.05 to 0.1 suns. Therefore, the most valuable Suns-V_{OC} data are during low-illumination periods of up to 0.1 suns, where the impact on system output is low. The Suns(M_{PP}) is likely to change slightly over time, which is a result of I_{SC} and/or I_{MP} degradation. A study of degradation rates of 12 different silicon modules found most severe I_{SC} and I_{MP} degradation of 0.71% and 0.89% annually.[31] These degradation rates correspond to a Suns(M_{PP}) increase of approximately 0.002 suns per year, or 0.05 suns over 25 years, for most modules in the CEC database. Therefore, Suns-V_{OC} might need to be monitored slightly beyond Suns(M_{PP}) to account for possible future degradation.

The simplest implementation is to measure temperature-corrected array V_{OC} from 0 suns to at least Suns(M_{PP}) and tracking it over time. This allows for monitoring the array before the start-up voltage for most inverters. Another simple implementation would be to track temperature-corrected DC voltage at maximum power (V_{MP}) against incident irradiance (Suns-V_{MP}).[32] This technique allows for data collection during normal M_{PP}-tracked system operation but does not remove the R_S contribution from resulting pseudo I-V curves. Comparison of Suns-V_{MP} and Suns-V_{OC} data allows R_S estimation and more advanced degradation analysis.

The operating temperature of a PV module undergoes rapid changes during sunrise and sunset, which corresponds to the light intensities of interest. For accurate temperature normalization, these temperature changes need to be accurately monitored, with special consideration given to the spatial distribution of module temperature. Non-uniform irradiance, wind conditions, and unmatched cell efficiencies may cause non-uniform temperature distribution.[33] The backsheet
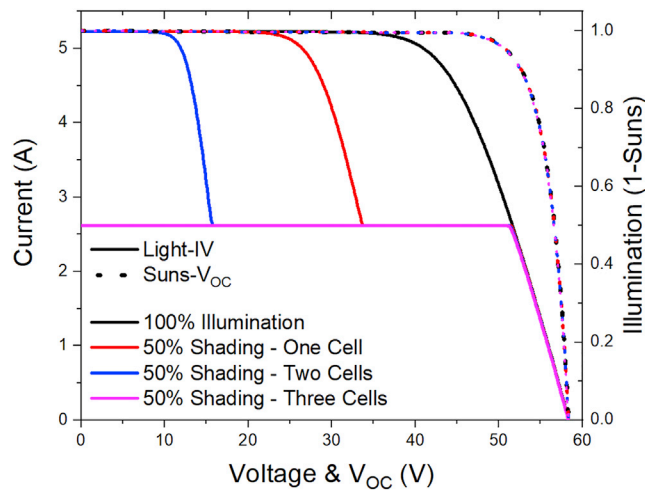
Figure 2. Simulated Shading Impacts on Light I-V and Suns-V_{OC} Curves
Simulated light I-V and Suns-V_{OC} curves of a 96-cell module using the equivalent solar cell circuit under four different illumination conditions; 100% illumination, 50% shading for a single cell, 50% shading for two cells within different strings, and 50% shading for three cells within different strings.

temperature was measured and used to calculate the cell temperature via Equation 3.[34] The V_{OC} was then normalized to a specific temperature using Equation 4.[35] Both Equations 3 and 4 are examined in more detail under the Experimental Procedures section.

$$T_{Cell} = T_{Backsheet} + (Suns \times 3°C) \qquad \text{(Equation 3)}$$

$$V_{oc} = \beta_0 + \beta_1 * \ln(Suns) + \beta_2 * T \qquad \text{(Equation 4)}$$

RESULTS AND DISCUSSION

Partial Shading Affects I-V but Not Suns-V_{OC}

Partial to near-complete shading complicates the analysis of module and array I-V curves. Bypass diodes create "stepped" I-V curves in partial shade; these stepped curves are typically filtered out when performing long-term analysis on large I-V curve datasets.[36] Here, we use LTspice (Linear Technology Corp) circuit modeling to demonstrate the stability of Suns-V_{OC} curves obtained from varying partial shade conditions that would otherwise generate erratic stepped I-V curves.[37]

A model was built of a 96-cell solar module comparable with those used in outdoor experimentation, as shown in Table 2. Individual PV cells were simulated based on a single-diode model, using R_S and R_{SH} values of 0.01 and 300 Ω, respectively.[38] Both I-V and Suns-V_{OC} measurements were simulated with various shading scenarios. Figure 2 shows modeled light I-V and Suns-V_{OC} curves for one-sun irradiance with 50% partial shading affecting one, two, and three cells, each from a different string.

The difference between the I-V and Suns-V_{OC} curves with zero shading is a manifestation of R_S. The steps found within the shaded simulations for the light I-V curve represent the activation of the bypass diodes. Bypass diodes are used in modules to prevent the formation of hot spots during periods of partial shade.[39] The bypass diodes only minimally impact the Suns-V_{OC} curves. When comparing the fully illuminated model to that of the three shaded cells, the pP_{MP} dropped by 0.2%, whereas the light I-V P_{MP} dropped by 35.5%.
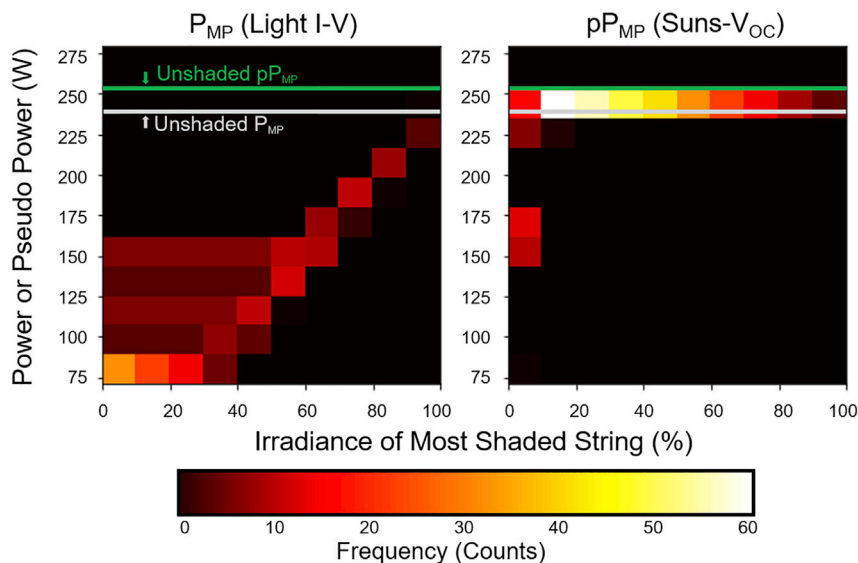
Figure 3. Simulated Shading Impacts on P_{MP} and pP_{MP}
Frequency histogram displaying maximum power (light I-V) and pseudo maximum power (Suns-V_{OC}) of a 3-string 96-cell module, under ~500 different partial shading conditions. String 1 and 2 are independently shaded from 0% to 100% illumination. String 3 is maintained at 100% illumination.

To further explore the stability of Suns-V_{OC} in widely varying partial shade conditions, we extend the 96-cell module LTspice model to include many different partial shade scenarios. These scenarios were created to demonstrate a wide range of possible partial shade conditions but are not necessarily reflective of real-world partial shading for a typical system. Figure 3 shows frequency histograms of the P_{MP} from I-V and pP_{MP} from Suns-V_{OC}, from roughly 500 different partial shade scenarios. Scenarios include shading affecting two of the three strings, from 0% (completely shaded) to 100% (fully illuminated), whereas string three is held at fully illuminated conditions. The x axis of Figure 3 corresponds to the shading level on the most shaded of the three strings.

As seen on the left side of Figure 3, P_{MP} varies substantially due to bypass diode activation and reduced light-generated current. For the given shading scenarios, the average of P_{MP} is 126 W with a standard deviation of 40.5 W. The right half of Figure 3 shows that Suns-V_{OC} pP_{MP} falls within a much more tightly distributed range, with an average of 238 W and a standard deviation of 25.7 W. Suns-V_{OC} provides a pP_{MP} within approximately 5% of the unshaded pP_{MP} when all strings are illuminated at values greater than ~5%. These results suggest that in systems that regularly operate in partial shade, I-V curves, or time-series P_{MP} data might rarely contain useful performance information. Considering diffuse irradiance is typically well over 5% of total illumination,[40] scenarios of less than 5% absolute illumination anywhere on the module are rare, even during periods of major shading. While true pP_{MP} requires uniform irradiance, a close estimate of pP_{MP} is obtained under almost all irradiance and shading conditions. Suns-V_{OC} curves frequently provide a value of pP_{MP} within 5% of the true unshaded pP_{MP}, providing a basis for robust time-series performance monitoring.

Outdoor Suns-V_{OC} Is Equivalent to Indoor Suns-V_{OC} Measurements
Outdoor Suns-V_{OC} data for a single-cell module are shown in Figure 4, with translations to 10°C, 25°C, and 40°C via Equation 4. Indoor Suns-V_{OC} measurements were also conducted at these respective temperatures using a Sinton FCT-450 cell flash
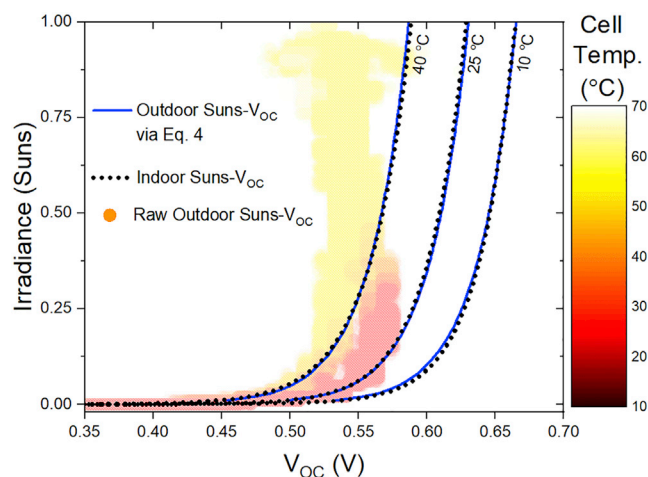
Figure 4. Temperature-Translated Outdoor Suns-V$_{OC}$ on Single-Cell Module
Temperature translation of outdoor Suns-V$_{OC}$ curves using Equation 4 compared with indoor Suns-V$_{OC}$ at 10°C, 25°C, and 40°C.

tester; these curves are also displayed in Figure 4. Temperatures of 25°C are used for standard test condition (STC) measurements, whereas 10°C and 40°C are used to demonstrate translations to lower and higher operating temperatures. Measured V$_{OC}$ datapoints are colored by cell temperature as determined from backsheet temperature measurements and Equation 3. Normalizing the measured outdoor data via Equation 4 to 10°C, 25°C, and 40°C yields an excellent agreement with the indoor curves. Suns-V$_{OC}$ parameters for each outdoor temperature translation are shown in Table 3, with the respective indoor parameters at the same temperature.

The pP$_{MP \text{ value}}$s of the temperature-translated outdoor Suns-V$_{OC}$ curves are within 0.04% of the respective indoor Suns-V$_{OC}$ curves, indicating the validity of our outdoor measurement setup and V$_{OC}$ translations via Equation 4. Slightly larger percentage differences occur when translating to 10°C. This is likely due to the paucity of data at such low temperatures for generating fit coefficients, considering the average outdoor operating temperature was approximately 35°C. Translating data to temperatures closer to the average operating temperature results in a more accurate fit. The specified translation temperature is best chosen given the average operating temperature of a given site or season.

The measurement error when comparing outdoor to indoor measurements must be less than the percentage of expected degradation to ensure viability. Modules are typically warrantied for ~1% degradation of maximum power per year. The measurement error for outdoor compared with indoor measurements equate to less than 0.04% error for

Table 3. Suns-V$_{OC}$ Parameters on a Single-Cell Module for Both Indoor and Normalized Outdoor Measurements

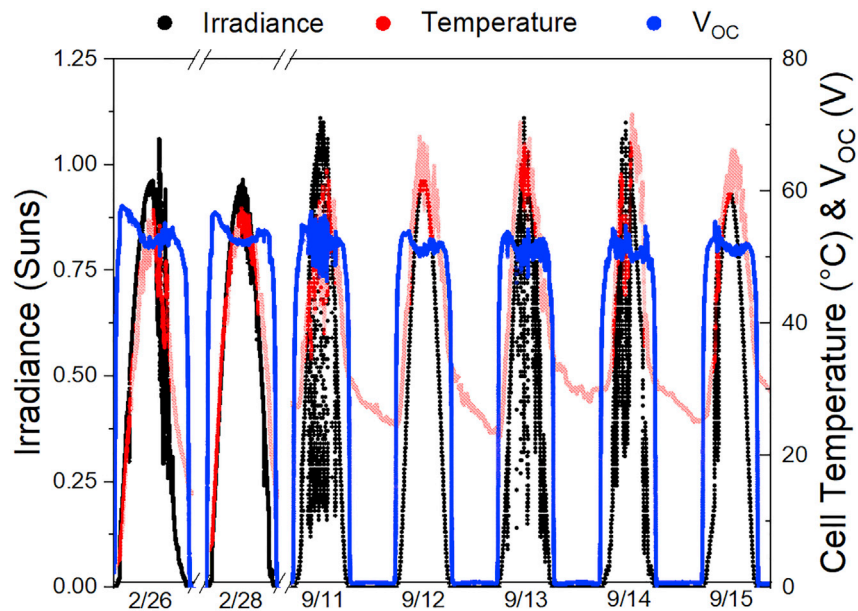|		R$_S$ (Ω-cm^2)	V$_{OC}$ at 1 Sun (V)	V$_{OC}$ at 0.1 Suns (V)	n	pFF	pP$_{MP}$ (W)
10°C	Indoor	2.89	0.665	0.603	1.00	0.834	4.71
	Outdoor	2.72	0.665	0.599	1.02	0.831	4.70
25°C	Indoor	2.95	0.629	0.563	1.11	0.821	4.39
	Outdoor	2.96	0.630	0.564	1.12	0.820	4.39
40°C	Indoor	3.01	0.589	0.519	1.27	0.803	4.02
	Outdoor	3.02	0.587	0.520	1.25	0.806	4.02

Figure 5. Raw Data for a 96-Cell Module

Solar irradiance, cell temperature, and measured V_{OC} for a 96-cell PV module located in Tempe, AZ, USA during February and September of 2019.

pP_{MP}, when analyzing using 25°C and 40°C for temperature translations. Because the measurement error is significantly less than the typical warrantied degradation, one should be able to use these data to make a reasonable assumption regarding rates of degradation.

Implementing Outdoor Suns-V_{OC} on Modules

Outdoor Suns-V_{OC} on one 96-cell module is shown in Figure 5. The data include irradiance, cell temperature, and measured V_{OC} from 2 days in northern hemisphere winter (February) and 5 days in autumn (September).

Each day was analyzed independently to quantify the variation introduced by daily and seasonal weather changes. Figure 6 shows each day's data individually translated to 40°C. Assuming the module had negligible degradation over this 6-month period, each day's Suns-V_{OC} curve should be similar. Daily $pP_{MP\ value}$s obtained across these days are listed in Table 4 and are within 1.3% of each other. Daily variations are roughly equal in magnitude to seasonal variations, indicating that the methodology is robust to seasonal weather variation.

Implementing a characterization technique on a large system must not interfere with normal power production. Potentially, Suns-V_{OC} data can be collected only during low irradiance periods at sunrise and sunset. Testing this hypothesis, the individual daily data displayed in Figure 6 were analyzed for both the full dataset and only considering data collected during sunrise and sunset (irradiance values <150 W/m^2), denoted as "SR & SS" in Table 4.

The results show that for daily changes, there is minimal variability when comparing the February data to the September data. The seasonal temperature extremes may cause the subtle differences found between seasons. September temperatures were approximately an average of 10°C warmer than February. Similar variability is observed when comparing full-day data to SR & SS-limited data. Temperature
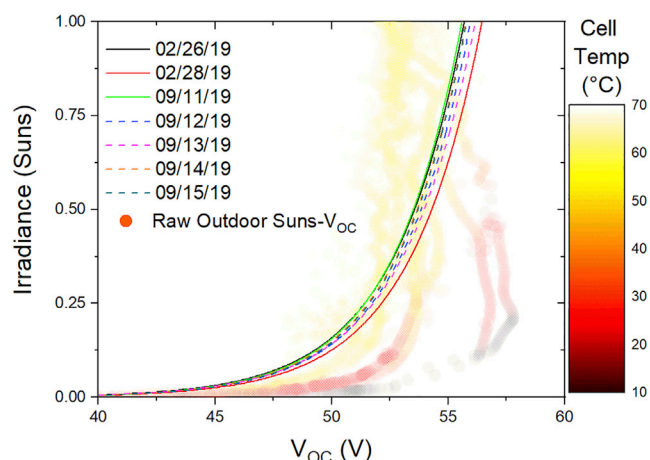
Figure 6. Temperature-Translated Outdoor Suns-V$_{OC}$ on 96-Cell Module
Outdoor Suns-V$_{OC}$ curves translated to 40°C for a 96-cell module; comparing seasonal and daily changes.

translations may also play a role in these differences; operating temperatures during low light intensity in the morning and evening are lower than the overall average operating temperature. The discrepancies between using data from the full day and only periods of low illumination are consistent from day to day, with relative average changes of 0.5% for V$_{OC}$, −0.9% for pFF, and 0.4% for pP$_{MP}$. Methodology should remain consistent to ensure parameters are analogous (e.g., low illumination only). These results suggest that Suns-V$_{OC}$ data collected daily, during periods of low illumination, resulted in stable metrics within a 1% range of variation. Analyzing longer time periods, such as weekly or monthly, averages out any day-to-day noise. True power measurements may have daily variances on the order of 10% to 20%, where Suns-V$_{OC}$ measurements are much more tightly distributed.

The data analyzed thus far have all used multiple temperature sensors attached to the backsheet and irradiance sensors positioned in plane, close to modules. This method is unrealistic when considering larger systems, where replacing temperature

Table 4. Suns-V$_{OC}$ Parameters on a 96-Cell Module Using Full Day versus SR & SS Irradiance Data

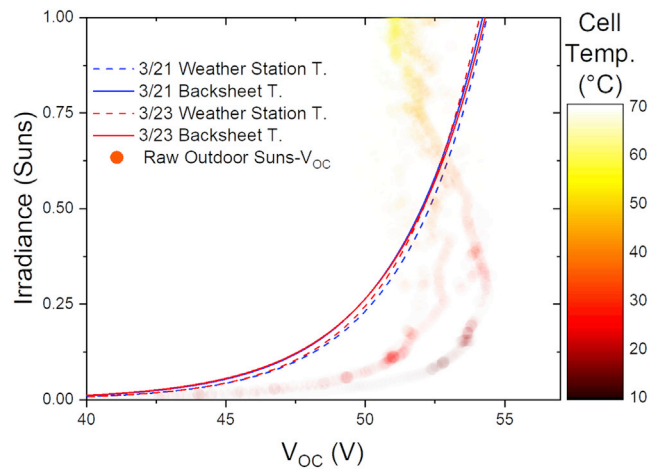|		V$_{OC}$ at 0.1 Suns (V)	pFF	pP$_{MP}$ (W)
2/26/2020	Full Day	48.58	0.809	235.7
	SR & SS	48.96	0.807	237.2
2/28/2020	Full Day	49.29	0.809	238.9
	SR & SS	49.59	0.806	240.2
9/11/2019	Full Day	48.67	0.812	236.1
	SR & SS	48.99	0.800	237.1
9/12/2019	Full Day	48.92	0.811	237.4
	SR & SS	49.21	0.799	238.3
9/13/2019	Full Day	48.88	0.807	237.0
	SR & SS	49.06	0.800	237.7
9/14/2019	Full Day	48.78	0.811	236.5
	SR & SS	49.01	0.803	237.4
9/15/2019	Full Day	48.83	0.812	236.9
	SR & SS	49.09	0.806	237.8

Figure 7. Weather Station versus Local Sensors for Outdoor Suns-V$_{OC}$
Suns-V$_{OC}$ curves translated to 40°C for a 96-cell module using measured backsheet temperature and weather station data.

and irradiance sensors with on-site weather station data is an alternative. Temperature translations on a 96-cell module were compared using both backsheet temperature sensors and local weather station data that included pyranometer plane of array (POA) irradiance, wind speed, and ambient air temperature. Equation 5 uses wind speed (WS), ambient temperature (T_a), and irradiance (E) to determine the backsheet temperature, where a and b are empirically determined coefficients.[34] We use a = −3.56 and b = −0.0750, corresponding to an open-rack polymer backsheet configuration.

$$T_{Backsheet} = E * e^{a + b*WS} * (T_a) \qquad \text{(Equation 5)}$$

2 days in March were used to compare measured backsheet temperature data with data captured from an on-site weather station. The weather station was positioned ~10 m away from the module, capturing data at a frequency of 1 min. Weather station sensors were ~2 m off the ground, where modules and their respective local sensors were ground mounted. When analyzing Suns-V$_{OC}$ using weather station data, the weather station POA irradiance was used instead of the local irradiance sensor. The resulting Suns-V$_{OC}$ curves, translated to 40°C, are displayed in Figure 7.

The results show slight inconsistencies during periods of low illumination, when using measured backsheet temperature compared with the weather station data. Using weather station data yields results in Suns-V$_{OC}$ curve translations within ±1% of the backsheet sensor translations. The largest differences occur in periods of low illumination. This is suspected to be due to rapid changes in operating temperature during low irradiance periods. Site-dependent determination of the empirical coefficients (a and b) used in Equation 5 could potentially yield more accurate results. Table 5 displays the Suns-V$_{OC}$ parameters, highlighting the slight discrepancies.

Results demonstrate that V$_{OC}$ and pFF are in good agreement when comparing the values obtained from measured backsheet temperature to those gathered exclusively using weather station data. In situations regarding large PV power plants, where implementation of individual temperature sensors is unrealistic, weather

Table 5. Suns-V_{OC} Parameters on a 96-Cell Module Using Measured Backsheet Temperature versus Weather Station Data
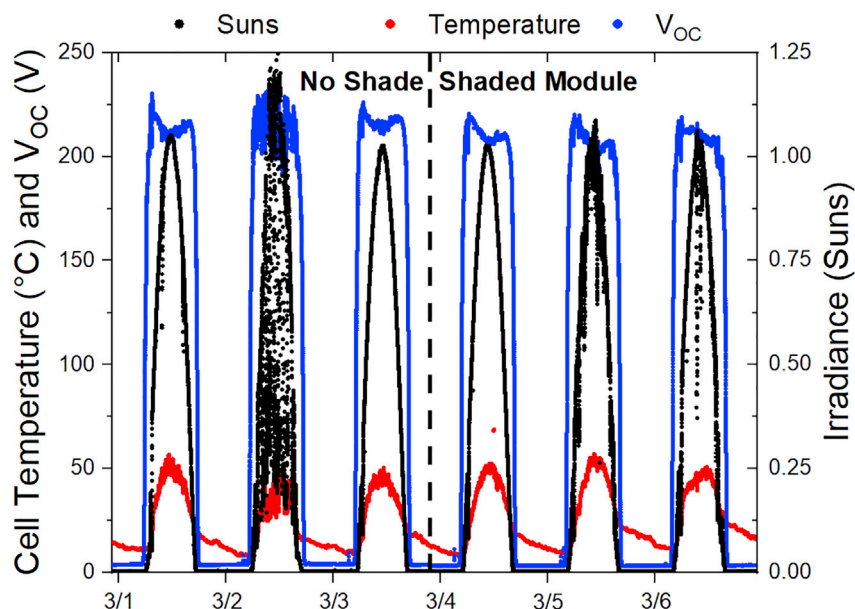
		V_{OC} at 1 Sun (V)	pFF	pP_{MP} (W)
3/21/2020	Backsheet	54.20	0.802	227.3
	Weather Station	54.36	0.807	229.4
3/23/2020	Backsheet	54.30	0.800	227.2
	Weather Station	54.10	0.806	228.1

station data can be used to estimate the module's operating temperature. Overall, across variations in day and season, with or without limiting data to low irradiance conditions, and using only on-site weather station data, Suns-V_{OC} results in stable metrics within a $\pm$ 1%–2% range of variation.

Implementing Outdoor Suns-V_{OC} on Arrays

A four-module array was analyzed in March 2020 for 6 days under split conditions. The first 3 days monitored the array's V_{OC} under unshaded conditions. For the last 3 days, one single module was artificially shaded at approximately 50% illumination by applying an opaque sheet on top of the surface of the module. Each module had three temperature sensors, totaling twelve sensors for the array. The irradiance was measured using a single irradiance sensor ~1 m from the array. The measured irradiance, operating temperature, and V_{OC} are displayed in Figure 8. The resulting Suns-V_{OC} curves of the array are displayed in Figure 9 for each day and translated to 40°C. Each day was independently analyzed to determine the resilience of shading effects on Suns-V_{OC}.

There is good agreement of the resulting Suns-V_{OC} curves between the 3 days of each respective split. When comparing the unshaded results with the shaded module results, there is a slight decrease in V_{OC}. This agrees with LTspice simulations,

Figure 8. Raw Data for a 4-Module Array
Solar irradiance, operating temperature, and measured V_{OC}, for a 4-module array with both full illumination and 50% partial shading on a single module.
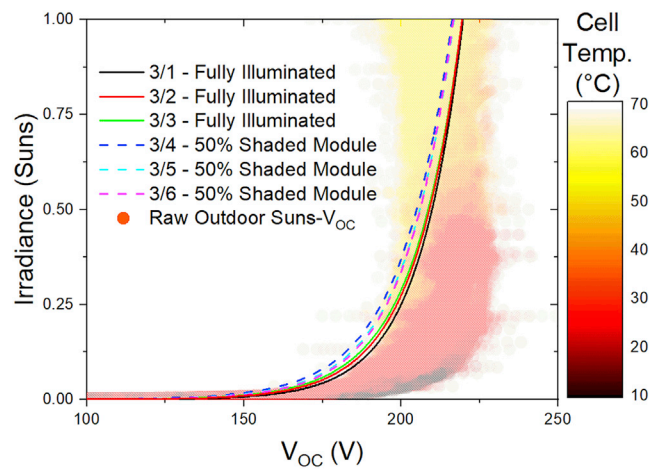
Figure 9. Temperature-Translated Outdoor Suns-V$_{OC}$ on 4-Module Array under Various Shading Conditions

Outdoor Suns-V$_{OC}$ curves of a 4-module array under normal illumination conditions and a 4-module array with one shaded module at 50% illumination conditions. March 1st to March 3rd are under normal illumination conditions. March 4th to March 6th are under shaded illumination conditions.

which suggest a 2–3 V drop in V$_{OC}$ when applying 50%–60% shading. The Suns-V$_{OC}$ parameters for each day are found in Table 6.

The extracted Suns-V$_{OC}$ parameters are almost identical for the 3-day splits. When comparing unshaded with shaded conditions, there is a noticeable, but expected drop in V$_{OC}$. The average delta in V$_{OC}$ is 2.9 V, which equates to a 3 mV drop in V$_{OC}$ for each cell in the shaded module. The ideality factor and pseudo FF are almost the same. These results suggest that Suns-V$_{OC}$ is resilient to significant levels of partial shading across arrays.

Implementing Outdoor Suns-V$_{OC}$ in the Real World

Outdoor characterization techniques must be able to accurately acquire data with minimal costs, little to no impedance on power production, and simplistic implementation in order to be effective. Implementation of these techniques may vary based on the system type and size, as small residential systems and large utility scale systems each present their own unique constraints.

In the United States, the average residential system size is 5 kW. These systems offer the advantage of having smaller string sizes, providing more resolution for Suns-V$_{OC}$ measurements. The disadvantage is that residential systems do not

Table 6. Suns-V$_{OC}$ Parameters on a 4-Module Array with Full Illumination versus ~50% Shading on a Single Module

Illumination Conditions	Date	V$_{OC}$ at 1 Sun (V)	n	pFF
100% illumination	3/1/2020	219.73	1.373	0.766
	3/2/2020	219.41	1.373	0.766
	3/3/2020	219.41	1.373	0.765
~50% shading on single module	3/4/2020	216.30	1.373	0.764
	3/5/2020	216.86	1.373	0.764
	3/6/2020	216.64	1.373	0.764

typically have on-site weather stations for measuring irradiance and temperature. Therefore, irradiance sensor(s) and temperature sensor(s) will need to be installed in strategic locations around the system. Multiple sensors may be needed if systems are installed with different tilt angles, though POA irradiance may be calculated from a single sensor.[41] Regarding data acquisition (DAQ), many commercially available data logger solutions currently exist. These data loggers can be placed between the PV and inverter to log data such as current, voltage, power, and peripheral weather sensors. These data loggers will acquire all the data needed to perform Suns-V_{OC} (open-circuit voltage) measurements before the inverter(s) reach their threshold voltage, as well as perform Suns-V_{MP} measurements after the inverter(s) have turned on. This configuration may not be adequate if the inverter threshold voltage is too low, resulting in irradiance levels too low for Suns-V_{OC} measurements. A simple DC controlled relay can be used to alleviate the issue caused by low inverter threshold voltages while an irradiance sensor can be used as the control for the relay, allowing the solar output to bypass to the inverter once the Suns-V_{OC} measurement has been conducted. For more advanced design, data loggers can be developed specifically for the purpose of conducting Suns-V_{OC} measurements on residential systems.

Utility scale systems offer more flexibility due to their larger system sizes and unique designs that may vary from powerplant to powerplant. An advantage for utility scale systems is that on-site weather stations are placed within the fielded modules. When designing an integrated outdoor Suns-V_{OC} system, one must consider the proximity of the weather stations to specific strings. If a weather station is placed too far from specific PV strings, irradiance and temperature data may not be an accurate representation for the respective strings. This can be problematic in instances of varying topography during low angle of incidences, such as sunrise and sunset, and during periods of partial shade from cloud coverage.

These powerplants may also deploy their own unique SCADA (Supervisory Control and Data Acquisition) systems to monitor and control their generation. Capturing Suns-V_{OC} data by use of the SCADA is unlikely because SCADA systems do not typically capture open-circuit voltage. However, SCADA systems may be used to capture Suns-V_{MP} data, without any new hardware.

Acquiring the open-circuit voltage measurements for Suns-V_{OC} will be largely dependent upon the desired resolution. When string-level resolution is desired, DAQ hardware can be placed within the combiner boxes. There are currently several commercially available monitoring devices, primarily used to monitor string voltages and currents. By placing the hardware within a combiner box, one DAQ can be used to monitor several different strings at the same time.

For higher monitoring resolution, such as individual modules, we can apply similar approaches to that of module-level power electronics (MLPE). DAQ hardware can be placed in parallel between individual modules, collecting open-circuit voltages at desired ranges of irradiance. An irradiance sensor can be used as a controller for when data should be collected, subsequently placing the module back in series with the string. This method is benefited by having localized irradiance measurements and more control precision, but it requires the use of an extra sensor. Contrasted to an irradiance sensor, the DAQ can simply be programmed to collect data by specific dates and times based on the respective sun positions. Using the date and time would not require an additional sensor, but it would need to be programmed individually based on the geographic coordinates. Finally, the module's

open-circuit voltage can be used for the DAQ shutoff threshold. This would be the simplest method to implement, yet, it would provide a more inconsistent operation. Degraded modules may take longer to reach this threshold voltage, consequently impeding the power production of the respective string. The approach of applying DAQ to individual modules can be used for both residential and utility installations, though utility installations may only sample a statistical representation of modules.

Conclusion

We show that Suns-V_{OC} can be applied outdoors on PV modules and arrays, providing much of the same useful diagnostic information as commonly found in indoor Suns-V_{OC}, including diode parameters free from the effects of series resistance. Collection of long-term PV performance data from light I-V curves is often impeded by logistical difficulties, variable weather, and the requirement to sweep I-V curves during major production hours of high, uniform irradiance. The results of this study prove that high-quality diagnostic parameters from Suns-V_{OC} can be performed during low irradiance conditions, perhaps even before the system voltage reaches the inverter start-up threshold. Suns-V_{OC} parameters derived from periods of exclusively using low irradiance, compared with using the entire range of irradiance, yield consistent relative deltas of 0.5% in V_{OC} at 0.1 suns, 0.9% in pFF, and 0.4% in pP_{MP}. If the data collection methodology is consistent, exclusively using low irradiance periods is valuable for monitoring changes over time. Outdoor Suns-V_{OC} is also robust against partial shading, meaning that instances of interrow self-shading will have minimal impacts on the Suns-V_{OC} parameters. Measurements can be expected to be within 5% of true pP_{MP} in nearly all partial shading conditions. In our outdoor measurements, we observe differences in performance metrics from daily and seasonal fluctuations produce maximum variations on the order $\pm 1\%$. Applications may include but are not limited to reliability studies, impeding fault detection, and performance monitoring.

We demonstrate the accuracy of temperature-translated outdoor Suns-V_{OC} compared with indoor measurements. For best accuracy, module temperature should be measured meeting requirements outlined by IEC 61583, and an appropriate cell temperature model should be applied. On-site weather station data comprised POA irradiance, ambient temperature, and WS, has proved to be an effective alternative to measuring the backsheet temperature and irradiance of each module; pP_{MP} results are within $\pm 1\%$ of the respective backsheet temperature results. With appropriate temperature translation, the parameters provided by Suns-V_{OC} curves taken in an outdoor setting may provide reliable degradation quantification and attribution without interfering with normal system operation.

EXPERIMENTAL PROCEDURES

Resource Availability

Lead Contact
Further information and requests for resources and materials should be directed to and will be fulfilled by the Lead Contact, Alex Killam (alexander.killam@asu.edu).

Materials Availability
This study did not generate new unique materials.

Data and Code Availability
The code generated during this study are available at Github, https://github.com/akillam1/Monitoring-of-Photovoltaic-System-Performance-Using-Outdoor-Suns-Voc

Materials

The Suns-V_{OC} technique was applied outdoors, using 3-string, 96-cell monocrystalline silicon Plurigas Solar Energias model BSM230 modules. Datasheet STC (AM1.5G, 25°C, 1,000 W/m^2) ratings of the panels are found in Table 2. Panels were ground mounted and arranged facing due south at a 33° tilt angle in Tempe, Arizona, USA.

Data Acquisition

To monitor the data, we used an AMT Mega328P microcontroller. A Texas Instruments ADS1115 provides the analog to digital data acquisition with 16 bits of resolution. We collected data approximately every 5 s for the system's V_{OC}, temperature sensors, and irradiance sensor. For experiments including the weather station, the data collection frequency was changed to every 60 s. This change was made so the data could be correlated with the weather station's reporting frequency. Decreasing the frequency of measurements may be conceivable, but less measurements will be possible during periods of rapid irradiance changes (i.e., sunrise and sunset). Therefore, a minimum 60 s frequency is advised to ensure accurate results when translating the raw data.

Irradiance Sensor

To measure irradiance, we measured the I_{SC} of a silicon solar cell positioned in plane with the array. It had the advantage of minimizing spectral mismatch effects between the sensor and array,[42] and by using similar encapsulant and glass on the sensor cell, we ensured similar irradiance changes from angle-of-incidence and soiling effects. As noted previously, irradiance accuracy is of secondary importance in Suns-V_{OC} measurements, so the calibration here is more stringent than needed. Indoor calibration against a reference cell gave a 99.97% coefficient of determination for the linearity of the irradiance sensor over the range of 0 to 1.2 suns. We validated the calibration outdoors against an NREL reference cell. The array is far from objects and shadows to minimize differences between the sensor cell and array (e.g., shadows cast on the irradiance sensor while the array is unshaded). The temperature dependence of the irradiance sensor is negligible due to the minor dependence of temperature on the short circuit current. Data presented here includes both days with intermittent scattered clouds and persistent overcast conditions.

Temperature Sensing and Normalization

To compensate for spatial nonuniformity, the module backsheet temperature was taken as the average of five temperature sensors, taped to the back of the module.[43] The module backsheet temperature is related to cell temperature via Equation 3, whereas 3°C corresponds to a glass/cell/polymer module mounted in an open-rack configuration.[34] Suns is the incident irradiance, expressed as a fraction, where 1 sun is equivalent to 1,000 W/m^2.

Measured V_{OC} attained at different cell temperatures must be normalized to one specific temperature for extraction of Suns-V_{OC} parameters. Equation 4 shows the relationship we use between V_{OC} and irradiance, where coefficients β_0, β_1, and β_2 are fit parameters, and T is the specified translation temperature.[44] β_0 is the fully illuminated V_{OC} at the specified temperature, β_1 is proportional to the thermal voltage at the specified temperature, and β_2 is the temperature coefficient of V_{OC} under fully illuminated conditions, assumed to be linear for all irradiance conditions. A least squares fitting algorithm was used to perform temperature translations with independent translations performed for each day of collected data. Initial guesses for each coefficient were as follows: the module's nameplate V_{OC} value was chosen

for β_0, the thermal voltage at the specified translation temperature multiplied by the total number of cells was chosen for β_1, and -0.0022 multiplied by the number of cells (change in V_{OC} per °C as calculated using empirical values for silicon) for β_2. Initial guesses are performed to enable more accurate fits. Translated results and discussion follows in section IV.

Extraction of Suns-V_{OC} Parameters

The collected raw data are initially filtered to remove any outliers using Isolation Forest Methodology.[45] This dataset is then translated to the desired temperature using procedures discussed in section D. The Suns-V_{OC} parameters are then extracted from the temperature-translated data. Open-circuit voltages in this work are reported at 1 and 0.1 suns and can be extracted by slicing the temperature-translated data at the respective irradiance value. As discussed earlier, V_{OC} at 0.1 suns corresponds to V_{MP} but without the effects of R_S. V_{OC} at ~0.1 suns can be directly used as a figure of merit for system performance and monitored over time. Alternately, it is possible to use the Suns-V_{OC} to extract more familiar diode parameters.

The derivative of V_{OC} with respect to the logarithm of the irradiance gives the diode ideality factor, as shown in Equation 6.

$$n = \frac{q}{kT} \frac{d\,V_{OC}}{d\,\ln(Suns)} \qquad \text{(Equation 6)}$$

While n be presented as a curve,[46] the most relevant metric for performance analysis is from 1 sun V_{OC} to 0.1 suns (corresponding to M_{PP}). Taking the slope from 0.1 to 1 suns also has the advantage of being less affected by noise than the tangent.

Further analysis gives pP_{MP} and pFF, which are the M_{PP} and FF, respectively, in the absence of RS. The pP_{MP} can be estimated, as shown in Equation 7, by equating suns to the system I_{SC}.

$$pP_{MP} = [(1 - suns) \times I_{SC} \times V_{OC}]_{max} \qquad \text{(Equation 7)}$$

For high resolution Suns-V_{OC} data, pFF can be calculated, as shown in Equation 8.

$$pFF = \frac{[(1 - suns) \times V_{OC}]_{max}}{V_{OC(0.1suns)}} \qquad \text{(Equation 8)}$$

However, outdoor field data usually have insufficient resolution to determine the maximum accurately, so we use n from Equation 6 to calculate pFF using Equations 9 and 10[47]:

$$pFF = \frac{v_{OC} - \ln(v_{OC} + 0.72)}{v_{OC} + 1} \qquad \text{(Equation 9)}$$

$$v_{OC} = \frac{q}{nkT} V_{OC} \qquad \text{(Equation 10)}$$

These two equations also assume a single ideality factor from V_{OC} to M_{PP}, and we can use the previously calculated value of n.

The temperature-translated parameters of V_{OC} at 1 and 0.1 suns, ideality factor, and pFF track each other, as shown in Tables 3, 4, 5, and 6. For a given system type, V_{OC} at 0.1 suns can be tracked directly, with changes in V_{OC} providing an early indication of system problems. The pFF can be similarly tracked and has the added advantage of comparison to the more familiar FF to identify losses caused by R_S.

AUTHOR CONTRIBUTIONS

Conceptualization, A.C.K. and J.F.K.; Methodology, A.C.K. and J.F.K.; Formal Analysis, A.C.K. and J.F.K., Investigation, A.C.K.; Resources, A.A. and S.G.B.; Data Curation, A.C.K. and J.F.K.; Writing – Original Draft, A.C.K., J.F.K., and S.G.B.; Writing – Review & Editing, A.C.K., J.F.K., A.A., and S.G.B.; Supervision, A.A. and S.G.B.; Funding Acquisition, S.G.B.

DECLARATION OF INTERESTS

The authors declare no competing interests.

REFERENCES

1. Rezk, H., Tyukhov, I., Al-Dhaifallah, M., and Tikhonov, A. (2017). Performance of data acquisition system for monitoring PV system parameters. Measurement 104, 204–211.

2. Firth, S.K., Lomas, K.J., and Rees, S.J. (2010). A simple model of PV system performance and its use in fault detection. Sol. Energy 84, 624–635.

3. French, R.H., Podgornik, R., Peshek, T.J., Bruckman, L.S., Xu, Y., Wheeler, N.R., Gok, A., Hu, Y., Hossain, M.A., Gordon, D.A., et al. (2015). Degradation science: mesoscopic evolution and temporal analytics of photovoltaic energy materials. Curr. Opin. Solid State Mater. Sci. 19, 212–226.

4. Meyer, E.L., and van Dyk, E.E. (2004). Assessing the reliability and degradation of photovoltaic module performance parameters. IEEE Trans. Rel. 53, 83–92.

5. Sinton, R.A., and Cuevas, A. (2000). A Quasi-steady-state open-circuit voltage method for solar cell characterization. Proceedings of the 16th European Photovoltaic Solar Energy Conference, pp. 1–4.

6. Jäger-Waldau, A. (2019). PV Status Report 2019. EUR 29938 EN (Publications Office of the European Union). https://op.europa.eu/en/publication-detail/-/publication/dfa5cde5-05c6-11ea-8c1f-01aa75ed71a1/language-en.

7. Meyers, B., Deceglie, M., Deline, C., and Jordan, D. (2020). Signal processing on PV time-series data: robust degradation analysis without physical models. IEEE J. Photovoltaics 10, 546–553.

8. Munoz, M.A., Alonso-García, M.C., Vela, N., and Chenlo, F. (2011). Early degradation of silicon PV modules and guaranty conditions. Sol. Energy 85, 2264–2274.

9. Deceglie, M.G., Silverman, T.J., Marion, B., and Kurtz, S.R. (2015). Real-time series resistance monitoring in PV systems without the need for I-V curves. IEEE J. Photovoltaics 5, 1706–1709.

10. Fertig, F., Krauß, K., and Rein, S. (2015). Light-induced degradation of PECVD aluminium oxide passivated silicon solar cells. Phys. Status Solidi RRL 9, 41–46.

11. Chen, R., Tong, H., Zhu, H., Ding, C., Li, H., Chen, D., Hallam, B., Chong, C.M., Wenham, S., and Ciesla, A. (2020). 83% efficient mono-PERC incorporating advanced hydrogenation. Prog. Photovolt. Res. Appl. 23, 1–9.

12. Wilterdink, H., Sinton, R., Hacke, P., Terwilliger, K., and Meydbray, J. (2016). Monitoring the recovery of c-Si modules from potential-induced degradation using suns-voc curves. IEEE 43rd Photovoltaic Specialists Conference (PVSC), 2752–2755.

13. Tsanakas, J.A., Vannier, G., Plissonnier, A., Ha, D.L., and Barruel, F. (2015). Fault diagnosis and classification of large-scale photovoltaic plants through aerial orthophoto thermal mapping. Proceedings of the 31st European Photovoltaic Solar Energy Conference and Exhibition, pp. 1783–1788.

14. Jordan, D.C., Deline, C., Kurtz, S.R., Kimball, G.M., and Anderson, M. (2018). Robust PV degradation methodology and application. IEEE J. Photovoltaics 8, 525–531.

15. Killam, A., and Bowden, S. (2017). Characterization of modules and arrays with suns Voc. IEEE 44th Photovoltaic Specialist Conference (PVSC), 2719–2722.

16. Forsyth, M.K., Mahaffey, M., Blum, A.L., Dobson, W.A., and Sinton, R.A. (2014). Use of the Suns-Voc for diagnosing outdoor arrays amp; modules. IEEE 40th Photovoltaic Specialist Conference (PVSC) 2014, 1928–1931.

17. Guo, S., Schneller, E., Walters, J., Davis, K.O., and Schoenfeld, W.V. (2016). Detecting loss mechanisms of c-Si PV modules in-situ I-V measurement. In Reliability of Photovoltaic Cells, Modules, Components, and Systems IX Society of Photo-Optical Instrumentation Engineers (SPIE) Conference Series., pp. 99380N.

18. Walters, J., Guo, S., Schneller, E., Seigneur, H., and Boyd, M. (2018). PV module loss analysis using system in-situ monitoring data. IEEE 7th World Conference on Photovoltaic Energy Conversion (WCPEC) (A Joint Conference of 45th IEEE PVSC, 28th PVSEC 34th EU PVSEC), pp. 2204–2208.

19. Nann, S., and Riordan, C. (1990). Solar spectral irradiance under overcast skies (solar cell performance effects). IEEE Conference on Photovoltaic Specialists 2, 1110–1115.

20. Nordmann, T., and Clavadetscher, L. (2003). Understanding temperature effects on PV system performance. 3rd World Conference onPhotovoltaic Energy Conversion, 2003. Proceedings of, Osaka 3, 2243–2246.

21. Kaldellis, J.K., Kapsali, M., and Kavadias, K.A. (2014). Temperature and wind speed impact on the efficiency of PV installations. Experience

obtained from outdoor measurements in Greece. Renew. Energy 66, 612–624.

22. King, D.L., Kratochvil, J.A., and Boyson, W.E. (1997). Measuring solar spectral and angle-of-incidence effects on photovoltaic modules and solar irradiance sensors. Conference Record of the Twenty Sixth IEEE Photovoltaic Specialists Conference, pp. 1113–1116.

23. Dirnberger, D., Blackburn, G., Müller, B., and Reise, C. (2015). On the impact of solar spectral irradiance on the yield of different PV technologies. Sol. Energy Mater. Sol. Cells 132, 431–442.

24. Andrews, R.W., and Pearce, J.M. (2013). The effect of spectral albedo on amorphous silicon and crystalline silicon solar photovoltaic device performance. Sol. Energy 91, 233–241.

25. Mani, M., and Pillai, R. (2010). Impact of dust on solar photovoltaic (PV) performance: research status, challenges and recommendations. Renew. Sustain. Energy Rev. 14, 3124–3131.

26. Bowden, S.B., Yelundur, V.N., and Rohatgi, A. (2002). Implied-Voc and suns-Voc measurements in multicrystalline solar cells. Proceedings of the 29th IEEE Photovoltaic Special Conference, pp. 371–374.

27. Bowden, S., and Rohatgi, A. (2001). Rapid and accurate determination of series resistance and fill factor losses in industrial silicon solar cells. Proceedings of the of the 17th European Photovoltaic Solar Energy conference, pp. 1802–1805.

28. Karas, J., Sinha, A., Buddha, V.S.P., Li, F., Moghadam, F., Tamizhmani, G., Bowden, S., and Augusto, A. (2019). Damp heat induced degradation of silicon heterojunction solar cells With Cu-plated contacts. IEEE J. Photovolt. 10, 153–158.

29. Kerr, M.J., Cuevas, A., and Sinton, R.A. (2002). Generalized analysis of quasi-steady-state and transient decay open circuit voltage measurements. J. Appl. Phys. 91, 399–404.

30. Blair, N., DiOrio, N., Freeman, J., Gilman, P., Janzou, S., Neises, T., and Wagner, M. (2018). System advisor model (SAM) general description (Version 2017.9.5). https://www.nrel.gov/docs/fy18osti/70414.pdf.

31. Smith, R.M., Jordan, D.C., and Kurtz, S.R. (2012). Outdoor PV module degradation of current-voltage parameters. Proceedings of the 2012 World Renewable Energy Forum., pp. 1–7.

32. Sun, X., Chavali, R.V.K., and Alam, M.A. (2019). Real-time monitoring and diagnosis of photovoltaic system degradation only using maximum power point-the Suns-Vmp method. Prog. Photovolt. Res. Appl. 27, 55–66.

33. Zhou, J., Yi, Q., Wang, Y., and Ye, Z. (2015). Temperature distribution of photovoltaic module based on finite element simulation. Sol. Energy 111, 97–103.

34. King, D.L., Boyson, E.W., and Kratochvil, J.A. (2004). Photovoltaic array performance model. http://www.mauisolarsoftware.com/MSESC/xPerfModel2003.pdf.

35. Wang, M., Liu, J., Burleyson, T.J., Schneller, E.J., Davis, K.O., French, R.H., and Braid, J.L. (2020). Analytic Isc–Voc method and power loss modes From outdoor time-series I–V curves. IEEE J. Photovolt. 10, 1379–1388.

36. Ma, X., Huang, W., Schnabel, E., Köhl, M., Brynjarsdóttir, J., Braid, J.L., and French, R.H. (2019). Data-driven I–V feature extraction for photovoltaic modules. IEEE J. Photovolt. 9, 1405–1412.

37. Guo, S., Ma, F.-J., Hoex, B., Aberle, A.G., and Peters, M. (2012). Analysing solar cells by circuit modelling. Energy Procedia 25, 28–33.

38. Khanna, V., Das, B.K., and Bisht, D. (2013). MATLAB/SIMELECTRONICS models based study of solar cells. Int. J. Renew. Energy Res. 3, 30–34.

39. Silvestre, S., Boronat, A., and Chouder, A. (2009). Study of bypass diodes configuration on PV modules. Appl. Energy 86, 1632–1640.

40. Kurtz, S.R., Myers, D., Townsend, T., Whitaker, C., Maish, A., Hulstrom, R., and Emery, K. (2000). Outdoor rating conditions for photovoltaic modules and systems. Sol. Energy Mater. Sol. Cells 62, 379–391.

41. Loutzenhiser, P.G., Manz, H., Felsmann, C., Strachan, P.A., Frank, T., and Maxwell, G.M. (2007). Empirical validation of models to compute solar irradiance on inclined surfaces for building energy simulation. Sol. Energy 81, 254–267.

42. Dunn, L., Gostein, M., and Emery, K. (2012). Comparison of pyranometers vs. PV reference cells for evaluation of PV array performance. 38th IEEE Photovoltaic Specialists Conference (PVSC), pp. 2899–2904.

43. Lu, Z.H., Song, Q., Li, S.Q., Yao, Q., and Othman, A. (2009). The effect of non-uniform illumination on the performance of conventional polycrystalline silicon solar cell. Proceedings of the ISES World Congress 2007 (Vol. I - Vol. V), pp. 1445–1448.

44. Wang, M., Ma, X., Huang, W.-H., Liu, J., Curran, A., Schnabel, E., Köhl, M., Davis, K., Brynjarsdóttir, J., Braid, J., and French, R.H. (2018). Evaluation of photovoltaic module performance using novel data-driven I-V feature extraction and suns-VOC determined from outdoor time-series I-V curves. 2018 IEEE 7th World Conference on Photovoltaic Energy Conversion (WCPEC) (A Joint Conference of 45th IEEE PVSC, 28th PVSEC & 34th EU PVSEC), pp. 778–783.

45. Liu, F.T., Ting, K.M., and Zhou, Z.-H. (2012). Isolation-based anomaly detection. ACM Trans. Knowl. Discov. Data 6, 1–39.

46. McIntosh, K., and Honsberg, C. (2000). The influence of edge recombination on a solar cell's. Iv Curve. 16th European Photovoltaic Solar Energy Conference. pp, 1651–1654.

47. Green, M.A. (1981). Solar cell fill factors: general graph and empirical expressions. Solid State Electron 24, 788–789.